Shape Effect of Carbon Nanovectors on Angiogenesis

Padmaparna Chaudhuri,[†] Rania Harfouche,[†,§] Shivani Soni,[†,§] Dirk M Hentschel,[‡] and Shiladitya Sengupta[†,*]

[†]Laboratory of Nanomedicine, BWH-HST Center for Biomedical Engineering and [‡]Renal Division, Department of Medicine, Brigham and Women's Hospital, Harvard Medical School. [§]These authors contributed equally to the paper.

ABSTRACT Physically diverse carbon nanostructures are increasingly being studied for potential applications in cancer chemotherapy. However, limited knowledge exists on the effect of their shape in tuning the biological outcomes when used as nanovectors for drug delivery. In this study, we evaluated the effect of doxorubicin-conjugated single walled carbon nanotubes (CNT-Dox) and doxorubicin-conjugated spherical polyhydroxylated fullerenes or fullerenols (Ful-Dox) on angiogenesis. We report that CNTs exert a pro-angiogenic effect *in vitro* and *in vivo*. In contrast, the fullerenols or doxorubicin-conjugated fullerenols exerted a dramatically opposite antiangiogenic activity in zebrafish and murine tumor angiogenesis models. Dissecting the angiogenic phenotype into discrete cellular steps revealed that fullerenols inhibited endothelial cell proliferation, while CNTs attenuated the cytotoxic effect of doxorubicin on the endothelial cells. Interestingly, CNT promoted endothelial tubulogenesis, a late step during angiogenesis. Further, mechanistic studies revealed that CNTs, but not fullerenols, induced integrin clustering and activated focal adhesion kinase and downstream phosphoinositide-3-kinase (PI3K) signaling in endothelial cells, which can explain the distinct angiogenic outcomes. The results of the study highlight the function of physical parameters of nanoparticles in determining their activity in biological settings.

KEYWORDS: carbon nanoparticles · carbon nanotubes · fullerenols · angiogenesis

T he promise of nanotechnology lies in the ability to engineer customizable nanoscale constructs with payloads such as chemotherapeutics, or targeting or imaging agents.[1,2] Interestingly, while the single-walled carbon nanotubes (CNT) have been extensively explored for biomedical applications such as drug delivery or as probes for imaging,[3−6] spherical fullerenes have had limited use in cancer chemotherapy resulting from inherent hydrophobicity. However, the recent discovery that water-soluble fullerene derivatives can cross cell membranes[7] has accelerated the interest in using fullerenes for diagnostic and therapeutic purposes.[8−12] Very recently, amphiphilic fullerene (buckysome) was explored as a vector for paclitaxel.[13] Furthermore, we demonstrated the novel application of water-soluble polyhydroxylated fullerene (fullerenol) in chemotherapeutic drug delivery to the tumor.[14]

While an increasing number of studies are focusing on the application of carbon nanostructures on cancer cells, their use in targeting angiogenesis,[15] a critical step in tumor progression,[16,17] has been limited. Furthermore, while recent reports have shown that the shape of nanoparticles have a major impact on their biological outcomes,[18,19] limited knowledge exists on the potential impact of the shape of carbon nanostructures for targeting angiogenesis. To explore this further, we studied the effects of doxorubicin-conjugated fullerenols and single walled carbon nanotubes, as models of nanoscale spheres or rods respectively, on angiogenesis.

RESULTS AND DISCUSSIONS

Engineering Carbon−Doxorubicin Nanostructures. We chose an established procedure for the synthesis of fullerenol, which generates between 16−24 hydroxyl groups on the fullerene cage (Figure 1a).[20] Synthesis of the pegylated fullerenol doxorubicin conjugate is outlined in Material and Methods section and in Supporting Information (Figure SI1−2). Total loading of doxorubicin was 296 ± 7 μg/mg of fullerenol as quantified by absorption spectroscopy (Figure SI3). While the theoretical dimension of a fullerenol particle was expected to be no greater than 5 nm, following pegylation and conjugation of doxorubicin, we observed that the fullerenols tend to form monodisperse aggregates in the narrow size range of 60−80 nm, as confirmed by dynamic laser light scattering (Figure SI3) and electron microscopy (Figure 1b), which could not be further reduced in size. Interestingly, while nanoparticles less than 5.5 nm have been reported to be cleared by the kidney,[21] larger pegylated nanoparticles less
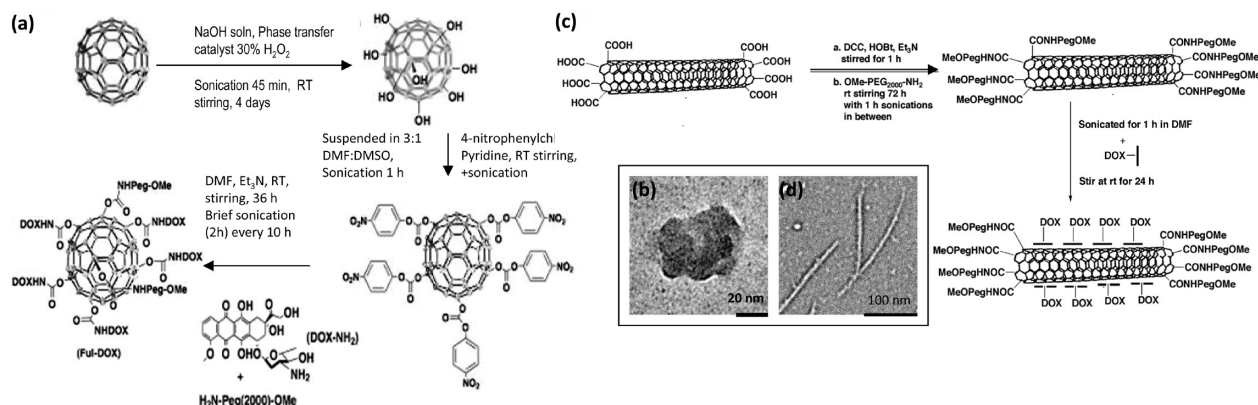
Figure 1. Synthesis of doxorubicin-conjugated fullerenol and CNTs. (a) Scheme depicting synthetic steps for fullerene functionalization and conjugation of doxorubicin (c) Scheme depicting synthetic steps for conjugation of PEG and attachment of doxorubicin to CNTs. Transmission electron micrographs show (b) doxorubicin-fullerenol and (d) doxorubicin-CNTs nanoparticles.

than 100 nm have been reported to preferentially target the tumors through leaky tumor neovasculature as a result of the enhanced permeability and retention (EPR) effect.[22] The unique size-range of the fullerenol aggregates therefore confers the functionality to preferentially home into the tumors as reported in our previous study.[14]

Carboxyl acid functionalized carbon nanotubes (length $500-1500$ nm, diameter $4-5$ nm) were oxidatively shortened by refluxing them in 3 M HNO_3.[23] The carboxyl acids were coupled to OMe-Peg(2000)-NH$_2$ *via* standard amide coupling protocol (Figure 1c). Pegylation improves blood circulation by decreasing opsonization and increasing the solubility of nanoparticles.[24] Doxorubicin was attached to CNT side-walls using the pyrene anchor. Pyrene being highly aromatic in nature is known to get irreversibly absorbed onto the inherently hydrophobic surfaces of CNT. It has been used as a universal anchor for attaching chemical and biological entities to CNT sidewalls and was used in the present study to attach doxorubicin to single-walled carbon nanotube (Figure 1b).[25] Doxorubicin was covalently attached to activated 1-pyrenebutanol *via* a carbamate linkage through its amine functionality (Figure SI6). Doxorubicin loading to the CNT was found to be between $285(\pm 40)$ μg/mg of the total nanoparticle weight. Transmission electron microscopy revealed that the particles were uniformly of $\sim$300 nm length (Figure 1d). The detailed synthesis procedure and the characterizations are provided in Material and Methods and Figures SI1—SI9.

Effect of Carbon Nanostructures on Angiogenesis *in Vivo*. To test the effect of CNT-doxorubicin and fullerenol—doxorubicin on angiogenesis *in vivo*, we harnessed a zebrafish embryo model. Angiogenesis from the subintestinal vessels can be easily visualized in the transparent zebrafish embryo, and as a result, it has emerged as a high-throughput *in vivo* system to screen for compounds that modulate angiogenesis.[26,27] Interestingly, treatment with CNT-doxorubicin induced angiogenesis *in vivo*, which was evident from the appearance of char-

acteristic angiogenic sprouts from the subintestinal vessel (Figure 2). In contrast, fullerenol—doxorubicin exerted a dose-dependent inhibition of angiogenesis, with complete ablation of angiogenic sprouts at 100 μM doxorubicin concentration (Figure 2). None of the treatments led to embryonic lethality or any gross morphological changes in the embryo.
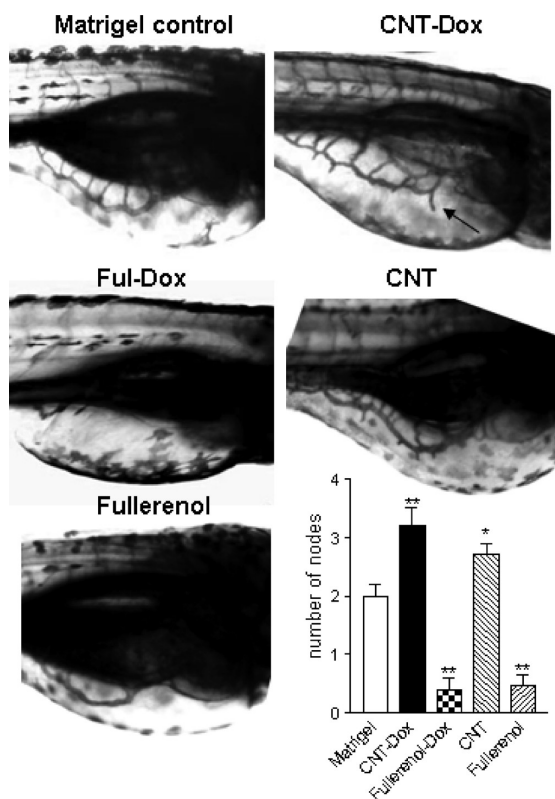

Figure 2. Effect of nanoparticle—doxorubicin conjugates on angiogenesis in embryonic zebrafish. The nanoparticles were injected in the yolk sac near the subintestinal vessels (SIV) of 48 hpf embryonic zebrafish and incubated for further 48 h. Images were taken after alkaline phosphatase staining in order to visualize the blood vessels. Arrow indicates the sprouting of neovasculature from SIV. Graphs show the morphometric quantification of the effects on the number of nodes. Data shown are mean $\pm$ SE ($n = 4-6$). *$P < 0.01$ *vs* matrigel alone control. (ANOVA followed by Newman Keul *post hoc* test).
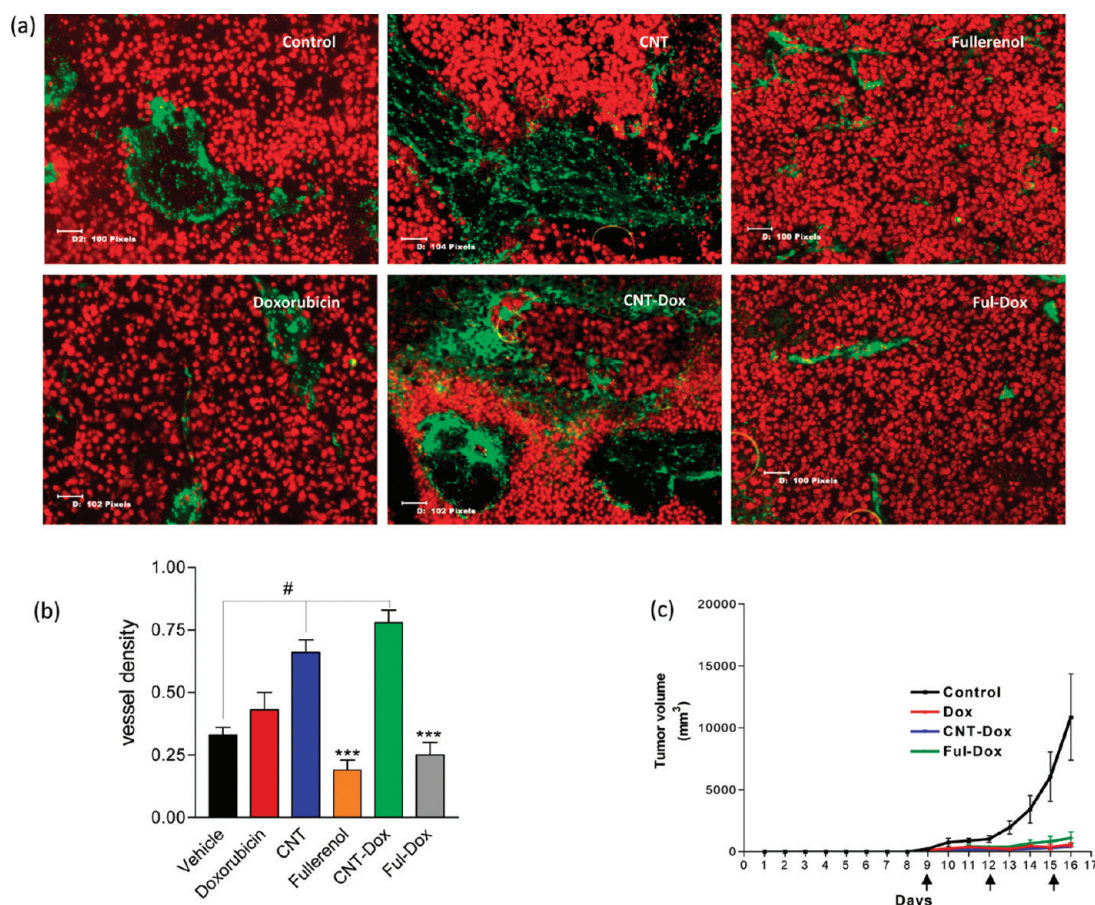
Figure 3. Effect of nanoparticle−doxorubicin conjugates on tumor angiogenesis. B16/F10 melanoma cells were implanted subcutaneously in the flanks of C57/BL/6 mice. Each group received three doses of the appropriate treatment every third day. (a) Tumor cryosections were immunolabeled with von Willebrand Factor (vWF) antibody and then probed with Alexa 488 conjugated secondary antibody. The sections were counterstained with propidium iodide. Images were captured with a Nikon Eclipse T*i* fluorescence microscope using QCapturePro software. Magnification = 10×. Scale bar is shown in pixels. One pixel = 0.45 μm. (b) Graph shows the morphometric quantification of vessels using ratio of green pixels (Alexa 488)/red pixels (PI). Data represent mean ± SE of $n \geq 6$: (#) $P < 0.05$, (∗∗∗) $P < 0.01$ (ANOVA followed by Newman Keuls *post hoc* test). (c) Effect of treatment on tumor growth. Arrows indicate the days of injection.

We next studied the effects of the carbon nanostructures in an *in vivo* syngeneic B16/F10 melanoma model, which is a highly vascularized tumor. Treatment was started when the tumors were 25 mm³ in volume, a stage where it is already vascularized,[28] and continued for three cycles, following which the tumors were excised and evaluated for the levels of vascularization. The tumor sections were immune-labeled for Von Willebrand factor (vWF), an endothelial cell marker (Figure 3a).[29] In this model, doxorubicin alone had no effect on tumor angiogenesis. In contrast, fullerenol−doxorubicin conjugate inhibited angiogenesis compared with vehicle-treated controls or doxorubicin alone. Interestingly, fullerenol alone also induced a significant inhibition of tumor angiogenesis as compared with vehicle-treated controls (Figure 3b), which can explain the reduction in tumor volume following fullerenol administration (Figure SI10). Tumor sections stained with hematoxylin and eosin (H&E) revealed highly vascularized tumors in the CNT-Dox treated group (Figure SI14), which was in keeping with the results obtained from vWF staining. Surprisingly, in

contrast to the fullerenol treatment and consistent with the observations made in the zebrafish assay, treatment with both CNT and CNT-doxorubicin significantly increased tumor angiogenesis as compared with vehicle-treated group. Interestingly however, CNT-doxorubicin exerted a similar tumor inhibition as compared with fullerenol−doxorubicin treatment (Figure 3c) despite the opposing effects on angiogenesis. This indicates that the EPR effect results in sufficient loading of the chemotherapeutic agent in the tumor to exert an antitumor outcome that overcomes the angiogenic effect.

Angiomodulatory Activity of Carbon Nanostructures on Cellular Processes Underlying Angiogenesis. To dissect the mechanisms underlying the opposite angiomodulatory activity of the carbon nanovectors, we harnessed two *in vitro* assays that mimic distinct steps during the angiogenesis process. In the presence of an angiogenic cue, endothelial cells lining the existing vasculature execute discrete sequential steps, including chemo invasion and migration through the basement membrane, cell proliferation and tubulogenesis.[16] As shown in Figure 4d,e,
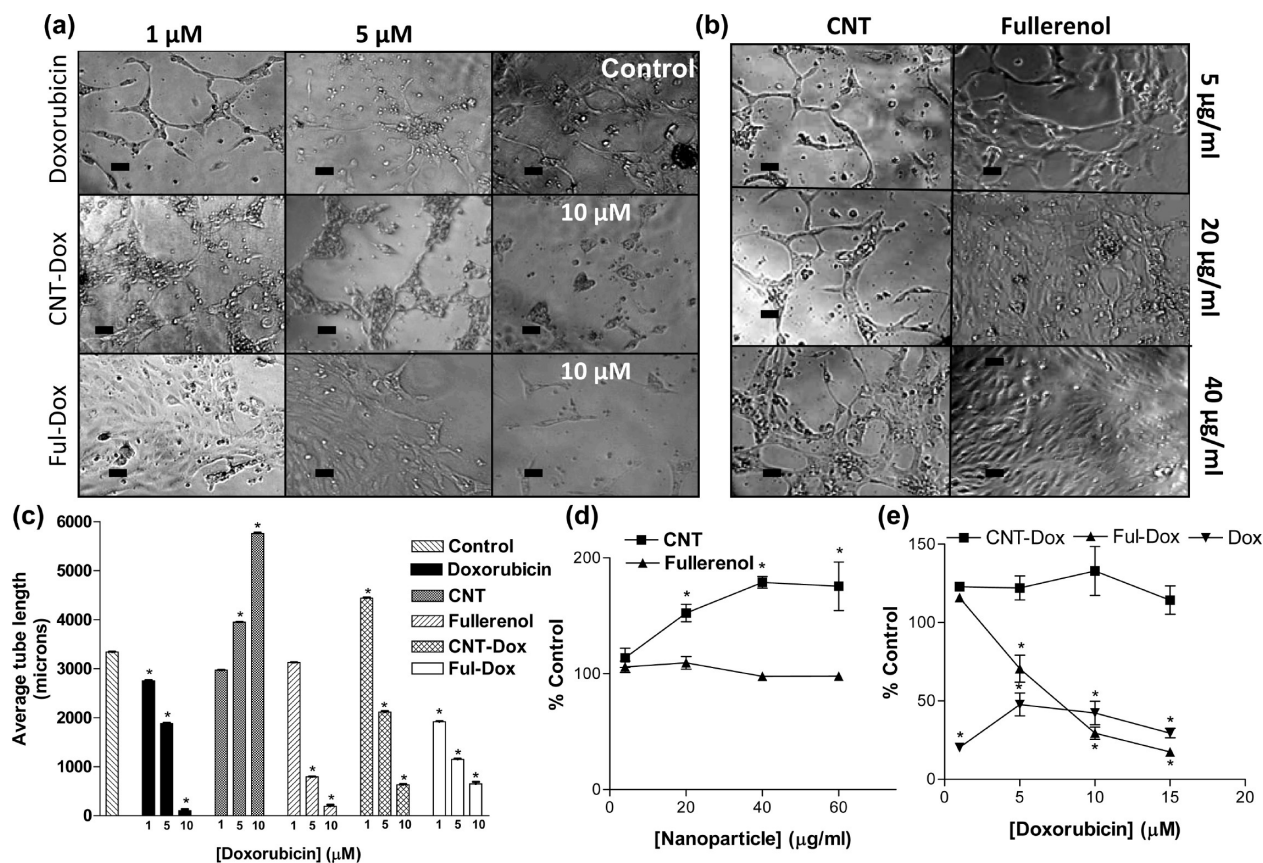
Figure 4. Effect of doxorubicin, nanoparticle—doxorubicin conjugates and empty nanoparticles on tubulogenesis and endothelial cell viability. Bright field images show the effect of (a) nanoparticle—doxorubicin conjugates or free doxorubicin and (b) empty nanoparticles on HUVECs tubulogenesis. Cells were plated on matrigel in 96-well plates. VEGF (5 nM) was added to each well after 24 h, and bright field images were obtained using a Nikon Eclipse TE 2000-U microscope using NIS-Elements AR 3.0 imaging software at 48 h. Magnification = 10×. Scale bar = 100 pixels. One pixel = 0.65 μm. (c) Graph shows average tube length in pixels. Data shown are mean ± SE from n = 5. Error signs are hidden under the bars: (∗) $P <$ 0.05 *vs* control. Effect of (d) empty nanoparticles and (e) nanoparticle—drug conjugates and free doxorubicin on endothelial cell viability. (∗) $P <$ 0.05 *vs* control (normalized to 100%) (ANOVA followed by Newman Keuls *post hoc* test).

treatment with the fullerenol—doxorubicin conjugate resulted in significant reduction in endothelial cell viability as compared with free doxorubicin, which can explain the *in vivo* observations. In contrast, CNT-doxorubicin conjugates exhibited no endothelial cell toxicity even at 15 μM concentration after 48 h treatment. Interestingly while treatment with pegylated CNT alone exerted a concentration-dependent increase in the cell proliferation (Figure 4d), fullerenols alone exerted no effect.

Proliferation of endothelial cells is followed by endothelial tubulogenesis, which precedes lumen formation. To test the effects of the carbon nanovectors on endothelial tubulogenesis, we used a well-characterized *in vitro* matrigel assay.[30] As shown in Figure 4a,c, doxorubicin alone induced a concentration-dependent inhibition of tube formation, although cytotoxicity was evident at concentrations greater than 5 μM. Interestingly, blank fullerenol also exerted a concentration-dependent inhibition of tube formation (Figure 4b,c) without affecting cell proliferation (Figure 4b). In contrast, CNTs alone induced a concentration-dependent increase in tubulogenesis (Figure 4b,c), and

conjugation of doxorubicin to the CNTs significantly attenuated the antitubulogenic effects of doxorubicin (Figure 4c), which can explain the pro-angiogenic effects observed in the *in vivo* studies. The failure of doxorubicin alone to significantly inhibit angiogenesis in the tumor model despite cytotoxicity to the endothelial cells *in vitro* could possibly arise from several pro-survival autocrine and paracrine survival signals between endothelial cells and matrix and tumor cells comprising the heterogeneous tumor environment. Indeed, in an earlier *in vitro* 3D-coculture study mimicking the *in vivo* tumor, we observed that doxorubicin failed to exert an antiangiogenesis effect.[31] The increased antiangiogenic potential of Ful-Dox probably arises from a sustained release of doxorubicin from the carbon fullerenol nanostructure, which exerts a "metronomic" antiangiogenesis effect.[32] Indeed, earlier studies have demonstrated that carbamate bond used in this study to conjugate doxorubicin to the carbon backbone of the fullerenes enables a sustained metronomic release of the active agent in tumor microenvironment.[14]

Modulation of Cell-Cycle by Carbon Nanostructures. To evaluate the mechanisms underlying the reduction in endo-
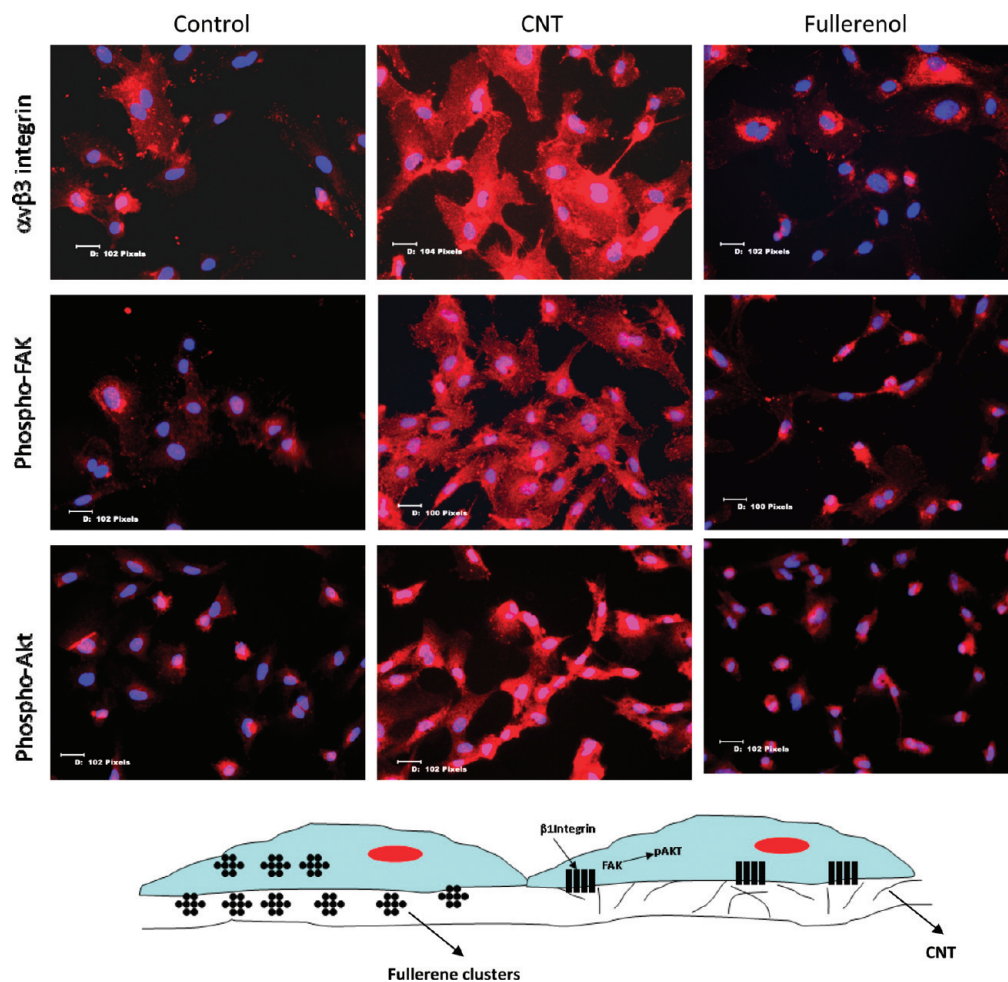
Figure 5. Effect of nanoparticle treatment on αvβ3 integrin expression, phosphorylation of FAK, and Akt by immunofluorescence. HUVEC treated with pegylated CNT and fullerenol were incubated with antibodies against αvβ3 integrin, phospho-FAK, and phospho-Akt and probed with Alexa 594-conjugated secondary antibody. Cells were counterstained with DAPI and images were captured with a Nikon Eclipse Ti fluorescence microscope using QCapturePro software. Magnification = 20×. Scale bar is shown in pixels. One pixel = 0.22 μm. Cartoon shows the mechanism through which the CNTs likely promote angiogenesis. The clustering of integrins results in phosphorylation of FAK, which can then activate Pi3kinase that phosphorylates Akt, which has been implicated in angiogenesis.

thelial cell viability seen with fullerenol−doxorubicin, we studied the effect of different treatments on the cell cycle. As shown in Figure SI11, treatment with free doxorubicin or fullerenol−doxorubicin conjugates for 24 h significantly reduced the percentage of cells in G1 stage as compared with vehicle-treated control, with an increased trend of cell cycle arrest in G2-M phase (Figure SI11). In contrast, there was no significant change in the CNT-Dox treated cells from the vehicle treated group. To further validate the observations, we elucidated the effect of the treatments on endothelial cell apoptosis. The cells were then probed with FITC-conjugated annexin-V, which binds to phosphatidylserine expressed on the outer membrane of apoptotic cells. The cells were counterstained with propidium iodide to label the DNA of late stage apoptotic or necrotic cells. As shown in Figure SI12 treatment with both doxorubicin and fullerenol−doxorubicin treatments resulted in a significantly higher percentage of cells in late apoptosis or necrosis stages as compared with control or

CNT−doxorubicin. No cell death was seen in the blank pegylated CNT and fullerenol. A potential rationale for the distinction in the susceptibility of the endothelial cells to CNT−doxorubicin and fullerenol−doxorubicin could arise from differences in cellular uptake. To explore this difference, we labeled the CNTs and fullerenols with FITC, and tracked their internalization into the cells and into the lysosomes through colocalization of the FITC-signal (green fluorescence) with Lysotracker Red (red fluorescence). Interestingly, we observed a rapid internalization of the fullerenols and localization within the lysosomal compartment within 2 h, in contrast, weak internalization was observed of the carbon nanotubes into HUVEC even at 8 h (Figure SI13), which could explain the differential susceptibility. This is an interesting observation and highlights the implications of shape of nanoparticles in modulating biological phenotype. This is consistent with recent literature reports. Indeed, Champion and Mitragotri demonstrated that wormlike particles with very high aspect ratios (>20)

exhibited minimal uptake into macrophages as compared to conventional spherical particles of equal volume.[33] This differential uptake was shown to be a result of local curvature of the particles at the points of contact.[34] Similarly, Geng *et al*. demonstrated that under fluid flow conditions, nanospheres and short flexible filaments are taken up by cells more readily than longer filaments because the latter are extended by the flow.[18] Again, in a report by Chan and co-workers, uptake of gold nanorods in HeLa cells was shown to be lower than gold nanospheres.[35] In contrast, Gratton *et al*. reported that rodlike particles enjoy an appreciable advantage when it comes to internalization rates in Hela cells, the efficiency of uptake being highly dependent on the aspect ratio of the particles.[36] Taken together, the results indicate that the shapes of nanostructures play critical roles in modulating their cellular uptake efficiencies, which differ significantly between specific cell types and determine their biological outcomes.

Mechanisms Underlying Pro-angiogenic Activity of CNTs. Although the differential uptake can explain the susceptibility of the endothelial cells to the nanovector-conjugated cytotoxic agent, it does not explain the pro-angiogenic effects seen with CNTs. To get a mechanistic insight into the pro-angiogenic effects of CNTs, HUVEC treated with pegylated carbon nanotubes was probed for expression and localization of $\alpha v\beta 3$ integrins, which has been implicated in angiogenesis.[37] As shown in Figure 5, treatment with CNTs resulted in an upregulation and reorganization (clustering) of the $\alpha v\beta 3$ integrins in the endothelial cells as compared to the vehicle-control cells or those treated with fullerenols. This is consistent with previous reports that have shown integrin upregulation and integrin-mediated cell spreading and stress fiber formation[38] that we see in the carbon nanotube-treated cells (Figure 5). A key mediator of integrin-mediated intracellular signaling cascade are the protein kinases such as focal adhesion kinase (FAK),[39] which was also found to be phosphorylated (activated) in carbon nanotubes-treated endothelial cells. Additionally, clustering of integrins at focal adhesions results in the activation of the PI3K-Akt pathway, which has been implicated in cell-survival and angiogenesis.[39] Indeed, Akt activation in the endothelial cells following CNT treatment was evident from increased levels of phospho-Akt in the CNT-treated cells. Collectively these results could explain the increased pro-angiogenic phenotype observed following treatment with CNTs. Interestingly, CNTs also at-tenuate the antitubulogenic effects of doxorubicin in the CNT-Dox conjugate, which explains the proangiogenic effect of the latter in the *in vivo* studies.

CONCLUSION

Carbon nanostructures are increasingly being studied for cancer chemotherapy or for imaging. Key advantages of carbon nanostructures as chemotherapeutic delivery agents lie in their structural homogeneity, increased drug loading efficiencies, defined shape, and size, with immense scope for chemical derivatization to the basic structure. Indeed, in this study, we observed significantly higher loading efficiency of the cytotoxic agent onto the carbon nanostructure backbone as compared to our previous studies using polylactide—polyglycolide-based nanoparticles.[40] However, despite similar chemical structures, carbon nanostructures come in many physical shapes and there is limited knowledge on the effect of their shape on biological outcomes. We demonstrate that carbon nanotubes exert a pro-angiogenic, mediated through the clustering of $\alpha v\beta 3$ integrins resulting in the activation of FAK and downstream PI3→Akt signaling pathways. It must however be noted that while this induces angiogenesis, the overall effect of CNT-Dox on tumor progression is still inhibitory, which can arise from a preferential accumulation in the tumor as a result of the EPR effect leading to cytotoxic effect on the tumor cells.[14] Interestingly, we observed that fullerenols failed to exert a similar clustering of integrins, and were rapidly internalized into the endolysosomal compartment. We have previously demonstrated that internalization can cause sustained release of the active agent, which can explain the increased antiangiogenic potential of Ful-Dox as compared with free doxorubicin. Indeed, it is now well established that a subcytotoxic but sustained concentration or metronomic dose of chemotherapeutic agents can exert antiangiogenesis effects.[32] These results, for the first time, demonstrate that carbon nanostructures can exert opposing effects on angiogenesis. Interestingly, the antiangiogenesis effect of polyhydroxylated fullerenes, ease of synthesis, their high water solubility, and advantage of high drug loading efficacy with preferential localization to the tumors, open up unique possibilities for the application of fullerenols as next generation delivery agents for anticancer drugs.

MATERIALS AND METHODS

Synthesis of Fullerenol and Fullerenol—Doxorubicin Conjugate. *Oxidation of Fullerene to Fullerenol.* A 2 ml portion of NaOH solution (1 g/mL) was added followed by 5—6 drops of 30% hydrogen peroxide solution and phase transfer catalyst tetrabutyl ammoniumhydrox-ide (40 wt. % solution in water) to a solution of sublimed C_{60} (Aldrich) in toluene (80 mg in 50 mL) and stirred vigorously for 5 days at room temperature. Formation of fullerenol was indicated by high water solubility of the formed solid, which caused transfer of color from the toluene layer to the aqueous phase. The

compound was precipitated out as a dark brown solid by the addition of ethanol to the water solution. The precipitate was washed with ethanol to remove excess reagent. Formation of OH groups was evident from a broad peak at 3400 cm^{-1} in FTIR.

Activation of Fullerenol. A homogeneous suspension of fullerenol (60 mg) in anhydrous dimethylformamide (DMF) was prepared by sonication, and *p*-nitrophenylchloroformate (400 mg), anhydrous pyridine (2 mL), and catalytic *N,N*-dimethylaminopyridine were added at 0 °C. The solution was allowed to stir for 48 h, under nitrogen, along with 1 h sonication every 8 h. Product formation was indicated by increased solubility in DMF. The brown solid was precipitated out by the addition of diethyl ether and washed with ether, dichloromethane and isopropyl alcohol, respectively. Product was characterized by aromatic doublets at 6.9 ppm and 8.2 ppm in proton NMR spectroscopy.

Attachment of Doxorubicin to Fullerenol. Activated fullerenol (5 mg) was dissolved in anhydrous DMF and sonicated under nitrogen for 30 min. Doxorubicin HCl (10 mg) was added at room temperature along with *N,N*-diisopropylethylamine and stirred for 10 min, after which OMe-Peg-NH$_2$ (M_w = 2000) (half molar equivalent with respect to Doxorubicin HCl) was added. The red solution was allowed to stir at room temperature under nitrogen for 30 h, with 1 h sonication every 8 h. A red solid was precipitated out by the addition of diethyl ether. The solid was washed with 1−2 drops of methanol in dichloromethane. The solid was dissolved in deionized water and dialyzed for 2 days against pure water (MWCO1000, SpectraPor). The solution was centrifuged at 5000*g* for 10 min to remove any aggregates and lyophilized to get the required compound as a dark red solid. The presence of conjugated doxorubicin was indicated by characteristic UV−visible absorbance spectra.

Synthesis of CNT and CNT-Doxorubicin Conjugate. *Oxidative Shortening and Purification of Single-Walled Carbon Nanotubes.* Oxidized single walled carbon nanotubes (Aldrich) (40 mg) were sonicated for 2 h in 3 M HNO$_3$ (100 mL) followed by 24 h reflux. The dark suspension was allowed to cool to room temperature and nanotubes were precipitated out by the addition of ethanol. The particles were washed with ethanol to remove any traces of the acid. The precipitate was then dissolved in deionized water and centrifuged at 1500*g* for 10 min. After discarding the precipitate, the solution was lyophilized to get particle lengths of ∼300 nm, in 35−40% yield.

Pegylation of Nanotubes. The resulting particles were dissolved in anhydrous DMF and sonicated for 1 h. 1,3-Dicyclohexyl-carbodiimide (DCC) and 1-hydroxybenzotriazole (HOBt) were added to the nanotubes, and the resulting black solution was stirred at room temperature for 10 min after which anhydrous triethylamine was added. Precipitation was observed as soon as the amine was added. This was followed by treatment with OMe-Peg-NH$_2$ (M_w = 2000) and 72 h room temperature stirring during which the precipitate dissolved completely. Diethyl ether was added to the solution to precipitate out a black solid, which was washed with ethanol and isopropyl alcohol to remove any excess reagents. Proton NMR study (δ = 3.01 ppm) and FTIR (amide C=O stretch, 1680 cm^{-1}) revealed the attachment of PEG *via* amide bond.

Synthesis of Doxorubicin−Pyrene Conjugate. To a solution of 1-pyrenebutanol (1 equiv) in anhydrous dichloromethane (Aldrich) and pyridine (4 equiv; Aldrich), *p*-nitrophenylchloroformate (2.5 equiv; Aldrich) was added at 0 °C. The reaction was stirred at room temperature for 5 h under N$_2$. The required compound was obtained as a pale yellow solid (75% yield) after column chromatographic purification. The product was characterized by mass spectrometry and NMR. Doxorubicin HCl (1 equiv) and the activated pyrene butanol (1.2 equiv) were stirred at room temperature in anhydrous DMF for 24 h in presence of anhydrous *N,N*-diisopropylethylamine. The resulting solid was purified by column chromatography using silica gel to obtain the pure product as a red solid in 60% yield. The compound was characterized by mass spectrometry. MALDI-TOF: calcd 843 (M), obtained 867 (M + Na)$^+$ and 883 (M + K)$^+$.

Attachment of Pyrene−Doxorubicin Conjugate to PEGylated Single-Walled Carbon Nanotube. Shortened carbon nanotubes (5 mg) were dissolved in DMF and sonicated for 1 h. The pyrene−doxorubicin conjugate (5 mg) was added to it and the resulting dark solution was further sonicated for 30 min. This was followed by room temperature stirring for 24 h. Diethyl ether was added to the so-

lution to precipitate out the solid. The solid was washed with dichloromethane with repeated centrifugation until the solution was free of any red color. Thin layer chromatography (TLC) indicated absence of any unattached pyrene−doxorubicin. UV−visible absorbance spectra of the obtained solid CNT−doxorubicin confirmed the presence of attached pyrene−doxorubicin.

Nanoparticle Characterization. High resolution TEM images were obtained on a JEOL 2011 high contrast digital TEM. For sample preparation, aqueous solutions of fullerenol−doxorubicin and SWCNT−doxorubicin were air-dried on carbon 300 mesh copper grids (Electron Microscopy Sciences). The size-distribution of fullerenol−doxorubicin clusters was confirmed with dynamic light scattering (DLS) (Malvern Nanozetasizer).

Cell Viability Assay. Human umbilical vein endothelial cells (HUVEC) were grown in Endothelial Basal Medium supplemented with EGM2 kit (Lonza). Cell cycle synchronized cells were seeded on 0.1% gelatin-coated 96-well plates (5000 cells/well), and treated with nanoparticle−doxorubicin conjugates or free doxorubicin at equivalent concentrations. Empty nanoparticle carriers at concentrations required to load the selected concentrations of doxorubicin were evaluated as controls. Cells were incubated in the presence of drugs for 48 h, washed with PBS, and cell viability was quantified using the MTS (CellTiter 96 Aqueous One Solution Cell Proliferation Assay; Promega) assay according to the manufacturers protocol and incubated at 37 °C. Absorbance of the bioreduced soluble formazan product was measured at 490 nm using a Versamax microplate reader. Results were quantified by manually subtracting the blank value from each value then normalizing against the control values.

Endothelial Tubulogenesis Assay. The 96-well plates were coated with 30 μL growth factor-reduced Matrigel (BD Biosciences, diluted 1:3 in PBS) per well. HUVECs (3 × 10^3 cells/well) were seeded in EBM containing 1% FBS along with the empty nanoparticles, nanoparticle-doxorubicin conjugates or free doxorubicin at appropriate concentrations (equivalent to 1, 5, 10 μM doxorubicin). After incubation for 24 h at 37 °C, 5 nM VEGF (Vascular Endothelial Growth Factor, R&D Systems) was added to each well and allowed to incubate for another 24 h. Bright field images were obtained after fixing with 4% PFA (paraformaldehyde) solution, using a Nikon Eclipse TE 2000-U microscope using NIS-Elements AR 3.0 imaging software.

Zebrafish Angiogenesis Assay. To assess the effect of CNT−doxorubicin and fullerenol−doxorubicin *in vivo*, we used a *Danio rerio* (zebrafish) embryo model. Zebrafish [TubingenAB] embryos were maintained at 28 °C in standard E3 solution buffered with 2 mM HEPES [(4-(2-hydroxyethyl)-1-piperazineethanesulfonic acid)]. At 48 h postfertilization embryos were anesthetized with Tricaine (0.04 mg/mL) and were dechorionated manually. The nanoparticles were diluted in matrigel and injected in the yolk sac near the sub-intestinal vessels (SIV) at a constant volume of 9.2 nL using a Nanoject II (Drummond Scientific).[41] Images were taken at 48 h postinjection both in real-time and after alkaline phosphatase staining using Nitroblue tetrazolium chloride and 5-bromo-4-chloro-3-indolyl phosphate toluidine salt in order to visualize the SIV vasculature. Bright-field imaging of the embryos was performed with a Nikon SMZ1500 stereomicroscope and SPOT Flex camera. The number of sprouts and the number of nodes from which the branches emerge in the SIV basket were measured for quantitative evaluation of angiogenesis. All procedures were approved by Harvard University IACUC (Institutional Animal Care and Use Committee).

Mouse Tumor Angiogenesis Model. B16/F10 melanoma cells (5 × 10^5) were implanted subcutaneously in the flanks of male C57/BL/6 mice (20 g, Charles River Laboratories). The animals were randomly divided into six treatment groups (each group containing eight mice) when the tumors attained volume of 25 mm^3; free doxorubicin, CNT− and fullerenol−doxorubicin conjugates, empty nanoparticles, and PBS control. Each animal was injected intravenous with 100 μL of nanoparticles equivalent to 6 mg/kg dose of free doxorubicin. The animals were sacrificed once tumor in the control groups reached 8000 mm^3. The tumors were harvested in OCT and cryofrozen. All animal procedures were approved by Harvard IUCAC. Tumors were cryosectioned (10 μm) and fixed in cold methanol at −20 °C. The tumor sections were probed with von

Willebrand Factor (vWF) antibody (Polyclonal rabbit, Dako) in blocking buffer. Sections treated after omitting the primary antibody or with an isotype antibody were used as negative controls. The tumor sections were then probed with Alexa 488 conjugated goat antirabbit secondary antibody (Molecular Probes), counterstained with PI and mounted using Prolong Gold Antifade Reagent (Molecular Probes). Images were captured using a using a Nikon Eclipse T*i* fluorescence microscope using QCapturePro software. The vessels were morphometrically quantified using ratio of green pixels (Alexa 488)/red pixels (PI). For histopathology studies, tumors were excised following animal sacrifice and the tissue blocks were fixed in 10% formalin solution then paraffin embedded, sectioned, and stained with hematoxylin and eosin (H&E) using the core facility of Harvard Medical School.

Cell Cycle Analysis. Synchronized cells, plated in 6-well plates (0.3×10^6 cells per well), were treated with free or nanoparticle−doxorubicin (10 μM doxorubicin equivalent), and incubated for 12 h. To release the cells from growth arrest, 5 nm VEGF was then added to the wells and incubated for additional 16 h. The cells were then trypsinized, collected over ice, and fixed with 70% cold ethanol (-20 °C for 30 min) to permealize the cell membrane. The cells were washed with PBS and stained with propidium iodide (PI) solution (50 μg/mL, containing RNase 1 mg/mL). The cell suspensions were transferred to FACS buffer and analyzed for PI staining on a BD FACS Calibur instrument. The data was analyzed using FloJo software.

Apoptosis Assay. Cells were incubated with nanoparticle−drug conjugates or free doxorubicin for 24 h, following which they were trypsinized, washed with PBS, and collected on ice. The cells were incubated with AnnexinV-Alexa Fluor 488 conjugate (Molecular Probes) and incubated in the dark at room temperature for 15 min. The cells were washed with PBS and counterstained with PI solution. The cell suspensions were then analyzed for AnnexinV/PI staining on a BD FACS Calibur instrument. Data were analyzed using a CellQuestPro software (BD Biosciences).

Cellular Uptake. To study the cellular internalization pathway of the nanotubes, HUVECs were seeded on glass coverslips in 24-well plates, 70000 cells per well. When cells reached ∼70% confluency, they were treated with fluorescein isothiocyanate (FITC) labeled carbon nanoparticles (CNT-FITC and Ful-FITC) for different durations of 2, 8, and 24 h, respectively. For colocalization studies, at indicated time points, the cells were washed with PBS and incubated with Lysotracker Red (Molecular Probes) at 37 °C for 30 min to allow internalization. The cells were fixed with 4% paraformaldehyde for 20 min at room temperature, then washed twice with PBS and mounted on glass slides using Prolong Gold Antifade Reagent (Molecular Probes). Images were obtained using a Nikon Eclipse T*i* fluorescence microscope using QCapturePro software equipped with green and red filters for FITC and Lysotracker Red, respectively.

Immunofluorescence Assay. HUVECs were grown on 0.1% gelatin-coated glass coverslips in 24-well plates with 70000 cells plated per well. When cells reached 70% confluency they were serum deprived (1% FBS in endothelial basal media) and incubated with pegylated carbon nanotubes and fullerenols at 20 μg/mL concentration for 24 h. Cells were fixed with 4% PFA and then treated with antihuman integrin $\alpha v \beta 3$ (R&D System), phospho-FAK(Tyr925) (rabbit, Cell Signaling Technology), and phospho-Akt(Ser473) (rabbit, Cell Signaling Technology) antibodies in blocking buffer at 4 °C overnight. Cells were probed with Alexa594 conjugated secondary antibodies (antimouse for integrin and antirabbit for FAK and Akt) from Molecular Probes. Cells were counterstained with DAPI and mounted using Prolong Gold Antifade Reagent (Molecular Probes). Images were captured using a using a Nikon Eclipse T*i* fluorescence microscope using QCapturePro software.

Statistics. All experiments were repeated at least three times with replicates, and data were expressed as mean ± SE. Data were tested using ANOVA, followed by Newman-Keuls *post hoc* test, with the level of significance set at $P < 0.05$.

REFERENCES AND NOTES

1. Ferrari, M. Cancer Nanotechnology: Opportunities and Challenges. *Nat. Rev. Cancer* **2005**, *5*, 161–171.
2. Peer, D.; Karp, J. M.; Hong, S.; Farokhzad, O. C.; Margalit, R.; Langer, R. Nanocarriers as an Emerging Platform for Cancer Therapy. *Nat. Nanotechnol.* **2007**, *2*, 751–760.
3. De la Zerda, A.; Zavaleta, C.; Keren, S.; Vaithilingam, S.; Bodapati, S.; Liu, Z.; Levi, J.; Smith, B. R.; Ma, T. J.; Oralkan, O.; *et al*. Carbon Nanotubes as Photoacoustic Molecular Imaging Agents in Living Mice. *Nat. Nanotechnol.* **2008**, *3*, 557–562.
4. Liu, Z.; Chen, K.; Davis, C.; Sherlock, S.; Cao, Q.; Chen, X.; Dai, H. Drug Delivery with Carbon Nanotubes for *in Vivo* Cancer Treatment. *Cancer Res.* **2008**, *68*, 6652–6660.
5. Bhirde, A. A.; Patel, V.; Gavard, J.; Zhang, G.; Sousa, A. A.; Masedunskas, A.; Leapman, R. D.; Weigert, R.; Gutkind, J. S.; Rusling, J. F. Targeted Killing of Cancer Cells *in Vivo* and *in Vitro* with EGF-Directed Carbon Nanotube-Based Drug Delivery. *ACS Nano* **2009**, *3*, 307–316.
6. Ajima, K.; Murakami, T.; Mizoguchi, Y.; Tsuchida, K.; Ichihashi, T.; Iijima, S.; Yudasaka, M. Enhancement of *in Vivo* Anticancer Effects of Cisplatin by Incorporation inside Single-Wall Carbon Nanohorns. *ACS Nano* **2008**, *2*, 2057–2064.
7. Foley, S.; Crowley, C.; Smaihi, M.; Bonfils, C.; Erlanger, B. F.; Seta, P; Larroque, C. Cellular Localization of a Water-Soluble Fullerene Derivative. *Biochem. Biophys. Res. Commun.* **2002**, *294*, 116–119.
8. Bakry, R.; Vallant, R. M.; Najam-ul-Haq, M.; Rainer, M.; Szabo, Z.; Huch, C. W.; Bonn, G. K. Medical Applications of Fullerenes. *Int. J. Nanomed.* **2007**, *2*, 639–649.
9. Cagle, D. W.; Kennel, S. J.; Mirzadeh, S.; Alford, J. M.; Wilson, L. J. *In Vivo* Studies of Fullerene-Based Materials Using Endohedral Metallofullerene Radiotracers. *Proc. Natl. Acad. Sci. U.S.A.* **1999**, *96*, 5182–5187.
10. Mikawa, M.; Kato, H.; Okumura, M.; Narazaki, M.; Kanazawa, Y.; Miwa, N.; Shinohara, H. Paramagnetic Water-Soluble Metallofullerenes having the Highest Relaxivity for MRI Contrast Agents. *Bioconjugate Chem.* **2001**, *12*, 510–514.
11. Ashcroft, J. M.; Tsyboulski, D. A.; Hartman, K. B.; Zakharian, T. Y.; Marks, J. W.; Weisman, B.; Rosenblum, M. G.; Wison, L. J. Fullerene (C60) Immunoconjugates: Interaction of Water-Soluble C60 Derivatives with the Murine Anti-gp240 Melanoma Antibody. *Chem. Commun.* **2006**, 3004–3006.
12. Zakharian, T. Y.; Seryshev, A.; Sitharaman, B.; Gilbert, B. E.; Knight, V.; Wilson, L. J. A Fullerene−Paclitaxel Chemotherapeutic: Synthesis, Characterization, and Study of Biological Activity in Tissue Culture. *J. Am. Chem. Soc.* **2005**, *127*, 12508–12509.
13. Partha, R.; Mitchell, L. R.; Lyon, J. L.; Joshi, P. P.; Conyers, J. L. Buckysomes: Fullerene-Based Nanocarriers for Hydrophobic Molecule Delivery. *ACS Nano* **2008**, *2*, 1950–1958.
14. Chaudhuri, P.; Paraskar, A.; Soni, S.; Mashelkar, R. A.; Sengupta, S. Fullerenol−Cytotoxic Conjugates for Cancer Chemotherapy. *ACS Nano* **2009**, *3*, 2504–2514.
15. Murugesan, S.; Mousa, S. A.; O'Connor, L. J.; Lincoln, D. W. 2nd; Linhardt, R. J. Carbon Inhibits Vascular Endothelial Growth Factor- and Fibroblast Growth Factor-Promoted Angiogenesis. *FEBS Lett.* **2007**, *581*, 1157–1160.
16. Folkman, J. Angiogenesis. *Annu. Rev. Med.* **2006**, *57*, 1–18.
17. Folkman, J. Tumor Angiogenesis: Therapeutic Implications. *New Eng. J. Med.* **1971**, *285*, 1182–1186.
18. Geng, Y.; Dalhaimer, P.; Cai, S.; Tsai, R.; Tewari, M.; Minko, T.; Discher, D. E. Shape Effects of Filaments *versus* Spherical Particles in Flow and Drug Delivery. *Nat. Nanotechnol.* **2007**, *2*, 249–255.

19. Champion, J. A.; Katare, Y. K.; Mitragotri, S. Particle Shape: A New Design Parameter for Micro- and Nanoscale Drug Delivery Carriers. *J. Controlled Release* **2007**, *121*, 3–9.

20. Kokubo, K.; Matsubayashi, K.; Tategaki, H.; Takada, H.; Oshima, T. Facile Synthesis of Highly Water-Soluble Fullerenes More than Half-Covered by Hydroxyl Groups. *ACS Nano* **2008**, *2*, 327–333.

21. Choi, H. S.; Liu, W.; Misra, P.; Tanaka, E.; Zimmer, J. P.; Ipe, B. I.; Bawendi, M. G; Frangioni, J. V. Renal Clearance of Quantum Dots. *Nat. Biotechnol.* **2007**, *25*, 1165–1170.

22. Maeda, H.; Bharate, G. Y.; Daruwala, J. Polymeric Drugs for Efficient Tumor-Targeted Drug Delivery Based on EPR Effect. *Eur. J. Pharm. Biopharm.* **2009**, *71*, 409–419.

23. Hirsch, A. Functionalization of Single-Walled Carbon Nanotubes. *Angew Chem. Int. Ed.* **2002**, *41*, 1853–1859.

24. Immordino, M. L.; Dosio, F.; Cattel, L. Stealth Liposomes: Review of the Basic Science, Rationale, and Clinical Applications, Existing and Potential. *Int. J. Nanomed.* **2006**, *1*, 297–315.

25. Chen, R. J.; Zhang, Y.; Wang, D.; Dai, H. Noncovalent Sidewall Functionalization of Single-Walled Carbon Nanotubes for Protein Immobilization. *J. Am. Chem. Soc.* **2001**, *123*, 3838–3839.

26. Serbedzija, G. N.; Flynn, E.; Willett, C. E. Zebrafish Angiogenesis: A New Model for Drug Screening. *Angiogenesis* **1999**, *3*, 353–359.

27. Childs, S.; Chen, J. N.; Garrity, D. M.; Fishman, M. C. Patterning of Angiogenesis in Zebrafish Embryo. *Development* **2002**, *129*, 973–982.

28. Folkman, J. Role of Angiogenesis in Tumor Growth and Metastasis. *Semin. Oncol.* **2002**, *29*, 15–18.

29. Zanetta, L.; Marcus, S. G.; Vasile, J.; Dobryansky, M.; Cohen, H.; Eng, K.; Shamamian, P.; Mignatti, P. Expression of von Willebrand Factor, An Endothelial Cell Marker, Is Up-Regulated by Angiogenesis Factors: A Potential Method for Objective Assessment of Tumor Angiogenesis. *Int. J. Cancer* **2000**, *85*, 281–288.

30. Ponce, M. L. Tube Formation: An *in Vitro* Matrigel Angiogenesis Assay. *Methods Mol. Biol.* **2009**, *467*, 183–188.

31. Sengupta, S.; Kiziltepe, T.; Sasisekharan, R. A Dual-Color Fluorescence Imaging-Based System for the Dissection of Antiangiogenic and Chemotherapeutic Activity of Molecules. *FASEB J.* **2004**, *18*, 1565–1567.

32. Kerbel, R. S.; Kamen, B. A. The Anti-angiogenic Basis of Metronomic Chemotherapy. *Nat. Rev. Cancer* **2004**, *4*, 423–436.

33. Champion, J. A.; Mitragotri, S. Shape Induced Inhibition of Phagocytosis of Polymer Particles. *Pharm. Res.* **2009**, *26*, 244–249.

34. Champion, J. A.; Mitragotri, S. Role of Target Geometry in Phagocytosis. *Proc Natl. Acad. Sci. U.S.A.* **2006**, *103*, 4930–4934.

35. Chithrani, B. D.; Ghazani, A. A.; Chan, W. C. W. Determining the Size and Shape Dependence of Gold Nanoparticles Uptake into Mammalian Cells. *Nano Lett.* **2006**, *6*, 662–668.

36. Gratton, S. E. A.; Ropp, P. A.; Pohlhaus, P. D.; Luft, J. C.; Madden, V. J.; Napier, M E.; DeSimone, J. M. The Effect of Particle Design on Cellular Internalization Pathways. *Proc. Natl. Acad. Sci. U.S.A.* **2008**, *105*, 11613–11618.

37. Avraamides, C. J.; Garmy-Susini, A.; Varner, J. A. Integrins in Angiogenesis and Lymphangiogenesis. *Nat. Rev. Cancer* **2008**, *8*, 604–617.

38. Su, Y.; Cui, Z.; Li, Z.; Block, E. R. Calpain-2 Regulation of VEGF-Mediated Angiogenesis. *FASEB J.* **2006**, *20*, 1443–1451.

39. Shiojima, I.; Walsh, K. Role of Akt Signaling in Vascular Homeostasis and Angiogenesis. *Circ. Res.* **2002**, *90*, 1243–1250.

40. Sengupta, S.; Eavarone, D. A.; Capila, I.; Zhao, G.; Watson, N.; Kiziltepe, T.; Sasisekharan, R. Novel Cancer Therapy Through Temporal Targeting of Both Tumor Cells and Neovasculature Using a Unique Nanoscale Delivery System. *Nature* **2005**, *436*, 568–572.

41. Nicoli, S.; Presta, M. The Zebrafish/Tumor Xenograph Angiogenesis Assay. *Nat. Protoc.* **2007**, *2*, 2918–2923.